

SUPPLEMENTAL MATERIAL

Supplemental Table

LQT3 Associated Mutation	Bisection Value of \hat{G}_{Na}	Final Value of \hat{G}_{Na}
Y1795C	N/A	1
I1768V	0.3058	0.1529
$\Delta K P Q$	0.0564	0.0282

Table S1. Mutant-specific relative sodium conductance scaling factor, \hat{G}_{Na} , for each mutation. Population variation of overall sodium conductance was applied by scaling mutant-specific relative sodium conductance \hat{G}_{Na} with individual scaling factor θ_{Na} . \hat{G}_{Na} values were calculated using a bisection algorithm to determine the maximum value that produced a mutant myocytes that repolarized in the baseline model (all other current conductances set to 1). The resulting value was then halved to such that the nominal value is not set at the threshold for repolarization. The mutant-specific \hat{G}_{Na} value was multiplied by the individual-specific scaling factor θ_{Na} and then baseline model sodium channel conductance (in units of mS/cm²) to set the overall sodium conductance for a given mutant and individual.

Supplemental Figures

Supplemental figures from the variable θ_{Na} population

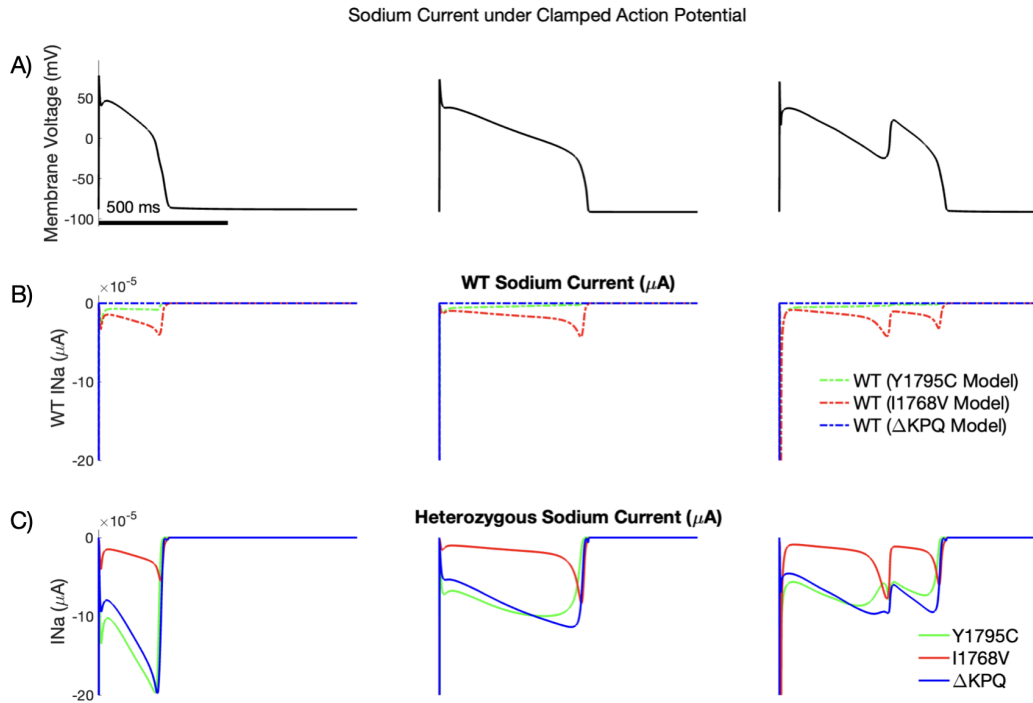


Figure S1. Current traces for the late component of the sodium current (I_{NaL}) using a clamped action potential (AP) under conditions of (left) healthy action potential duration (APD), (middle) prolonged APD, and (right) prolonged APD with the occurrence of an early after depolarization (EAD). Each column shows: (A) the AP morphology, (B) wild-type (WT) sodium current, and (C) the heterozygous mutant sodium current. There is a noticeable difference between the I_{NaL} amplitude of the Y1795C and Δ KPQ mutations and that of the I1768V mutation, as the I1768V I_{NaL} amplitude is lower than that of the other two mutations. For the prolonged action potential (middle), the I1768V mutation exhibits reactivation, resulting in a current amplitude increase in the late AP repolarization phase, whereas Y1795C and Δ KPQ exhibit a decrease in current amplitude. All mutations show increased I_{NaL} during late repolarization for the healthy APD.

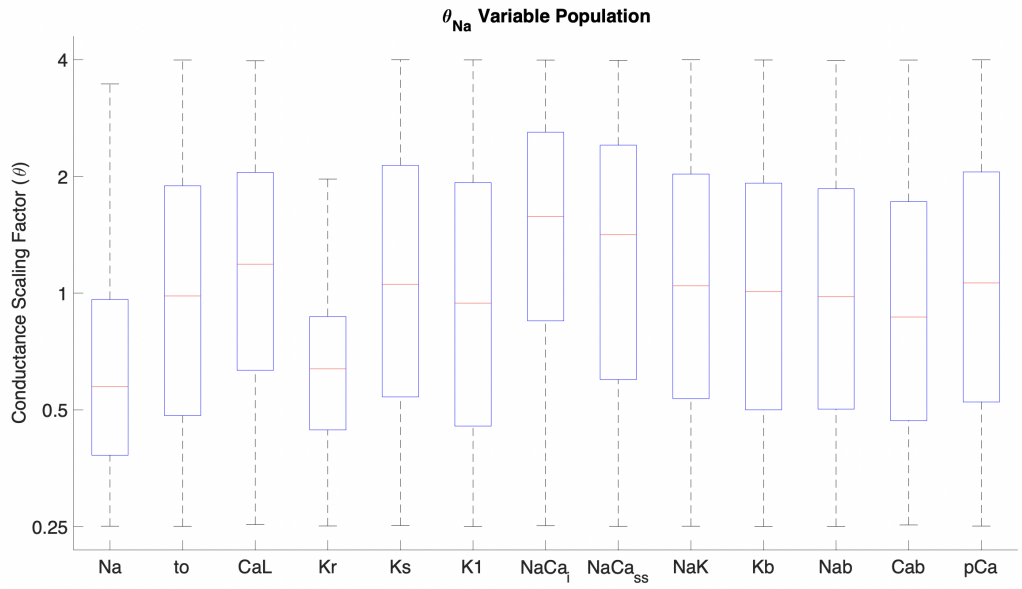


Figure S2. Distribution of ion current conductance scaling factors for the θ_{Na} variable population.

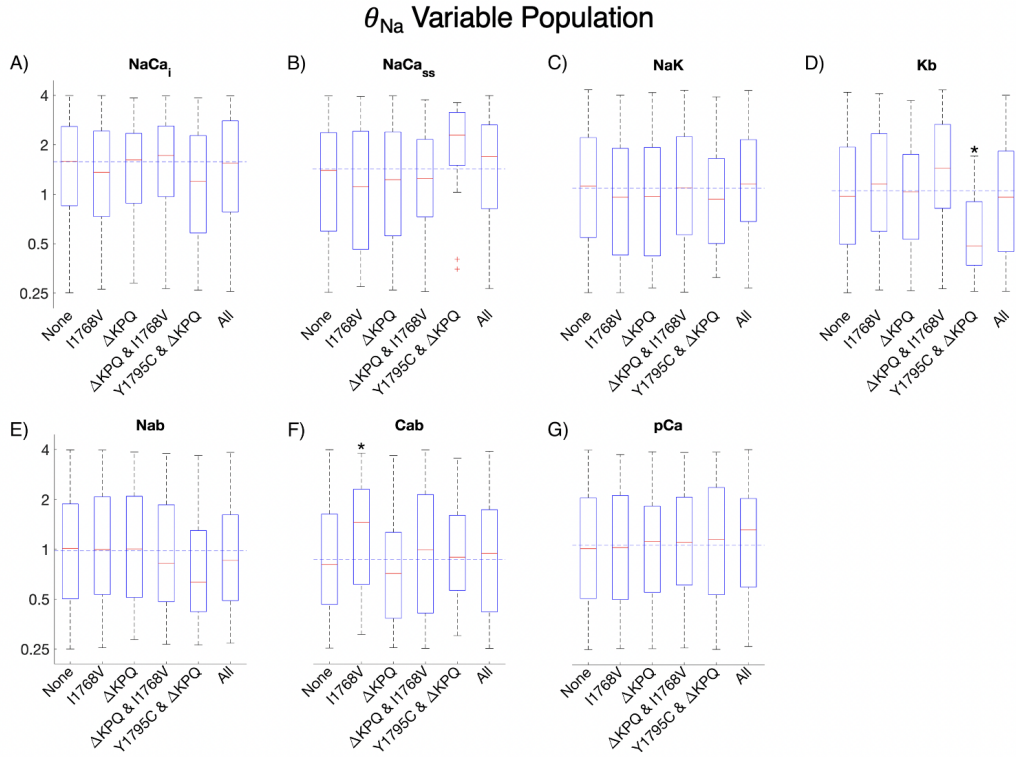


Figure S3. Relationship of conductance and susceptibility in θ_{Na} variable population, plotted on a logarithmic scale. Trends are shown for currents not included in the main text. Significance is in reference to the sub-population of cells susceptible to no mutation. Distribution of conductance coefficient for I_{NaCa_i} , $I_{NaCa_{ss}}$, I_{NaK} , I_{Nab} , and I_{pCa} corresponding to (A), (B), (C), (E), and (G), respectively, show no significant difference between susceptible and non-susceptible sub-groups. Cells susceptible to Y1795C and ΔKPQ but not I1768V have lower I_{Kb} conductance (D). Cells susceptible to I1768V only have a higher than normal conductance of I_{Cab} (F).

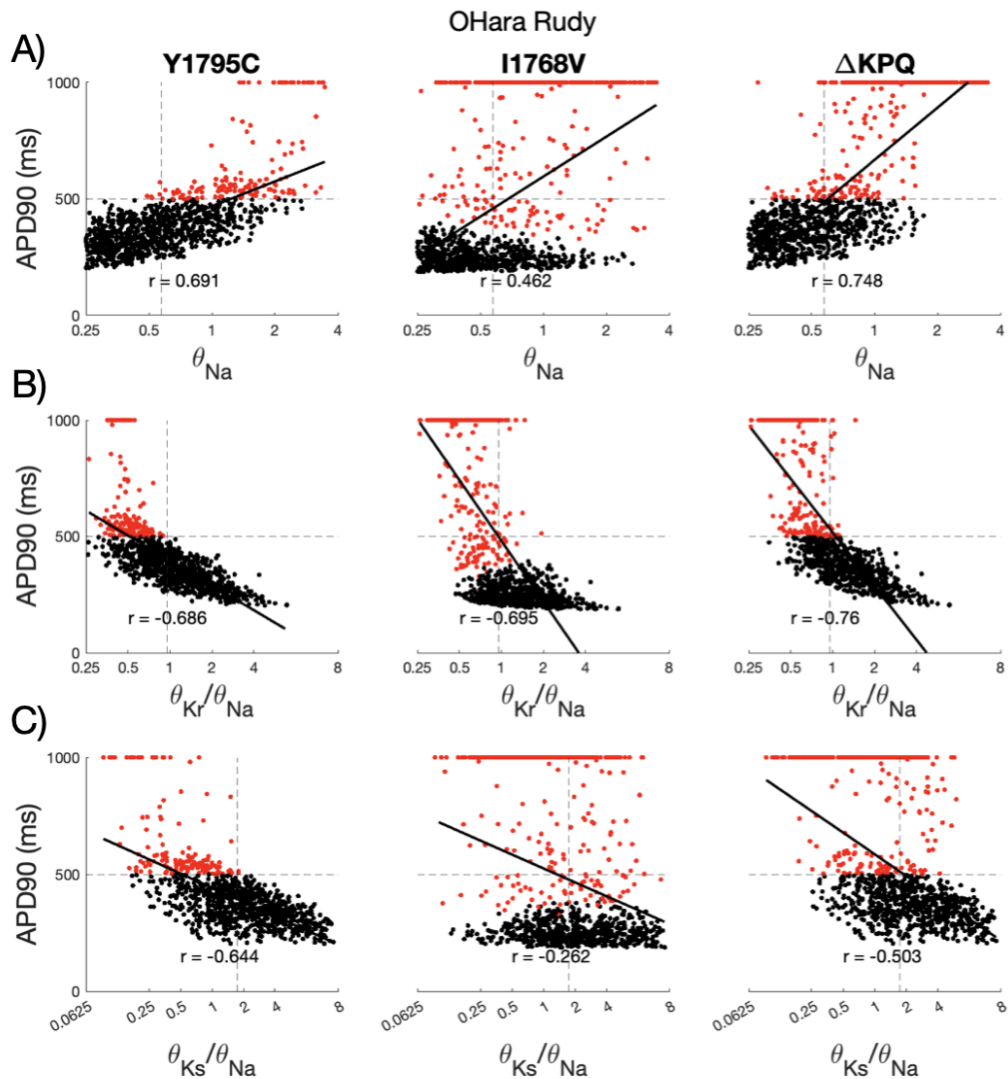


Figure S4. Correlation between major channel conductances and APD90 in virtual cells modeled with the O'Hara Rudy model. (A) APD90 dependence on θ_{Na} shows a strong positive correlation in Y1795C and ΔKPQ , but not in I1768V. (B) The $\theta_{Kr}-\theta_{Na}$ ratio has a stronger correlation with APD90, compared with θ_{Na} alone for cells with the I1768V mutation, while comparable correlations were observed in Y1795C and ΔKPQ . (C) In contrast, the correlation between the $\theta_{Ks}-\theta_{Na}$ ratio and APD90 is weak for both I1768V and ΔKPQ , with comparable correlation as the $\theta_{Kr}-\theta_{Na}$ ratio and θ_{Na} alone for Y1795C. Horizontal dashed line shows the APD90 threshold for cells to be considered susceptible to a mutation. Vertical dashed line indicates the median value of θ_{Na} , θ_{Kr}/θ_{Na} , and θ_{Ks}/θ_{Na} in A-C, respectively. Pearson's correlation coefficient (r) is shown, with the line of best fit shown in solid black.

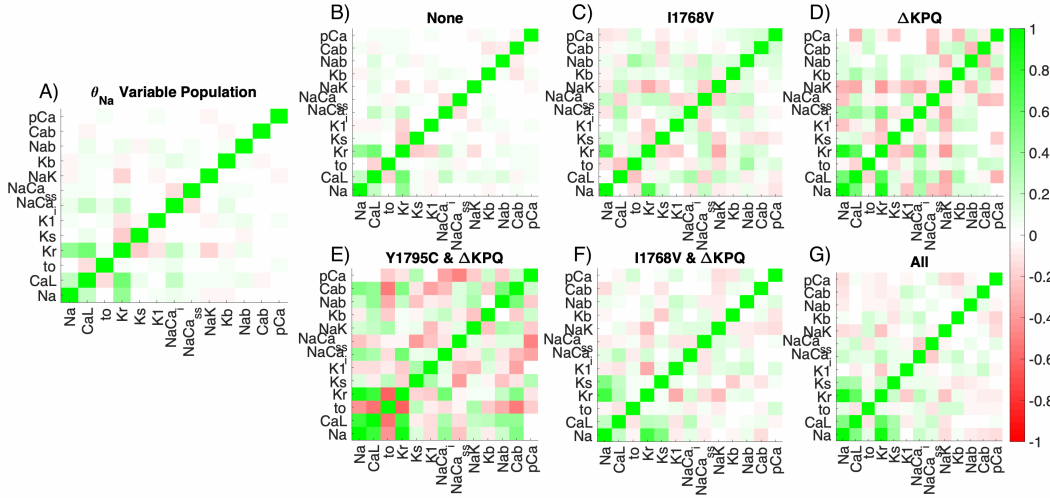


Figure S5. Pearson's correlation coefficient between pairs of all varied current conductances in the θ_{Na} variable population. Dark red indicates a strong negative correlation, lack of color (white) indicates no correlation, and bright green indicates strong positive correlation. Correlation coefficients between current conductance for (A) the whole generated population, (B) cells susceptible to no mutations, (C) cells susceptible to I1768V only, (D) cells susceptible to ΔKPQ only, (E) cells susceptible to Y1795C and ΔKPQ , (F) cells susceptible to I1768V and ΔKPQ , and (G) cells susceptible to all mutations.

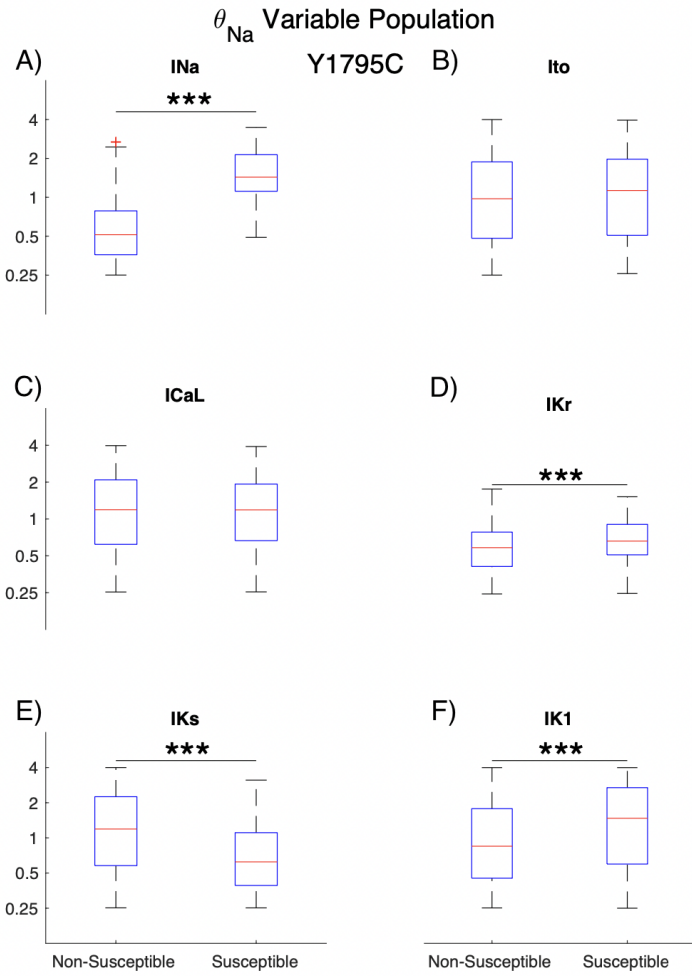


Figure S6. Boxplot illustrating difference in conductance scaling factor distributions for major currents, for the Y1795C mutation from the θ_{Na} variable population. We observe significant differences between susceptible and non-susceptible cells for θ_{Na} , θ_{Kr} , θ_{Ks} , and θ_{K1} .

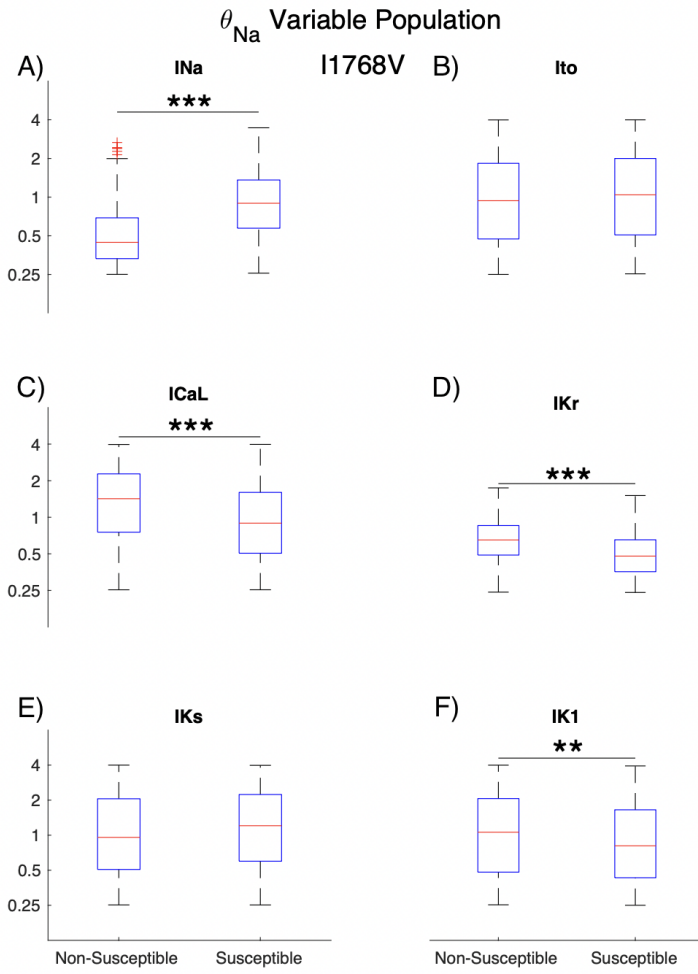


Figure S7. Boxplot illustrating difference in conductance scaling factor distributions for major currents, for the I1768V mutation from the θ_{Na} variable population. We observe significant differences between susceptible and non-susceptible cells for θ_{Na} , θ_{CaL} , θ_{Kr} , and θ_{K1} .

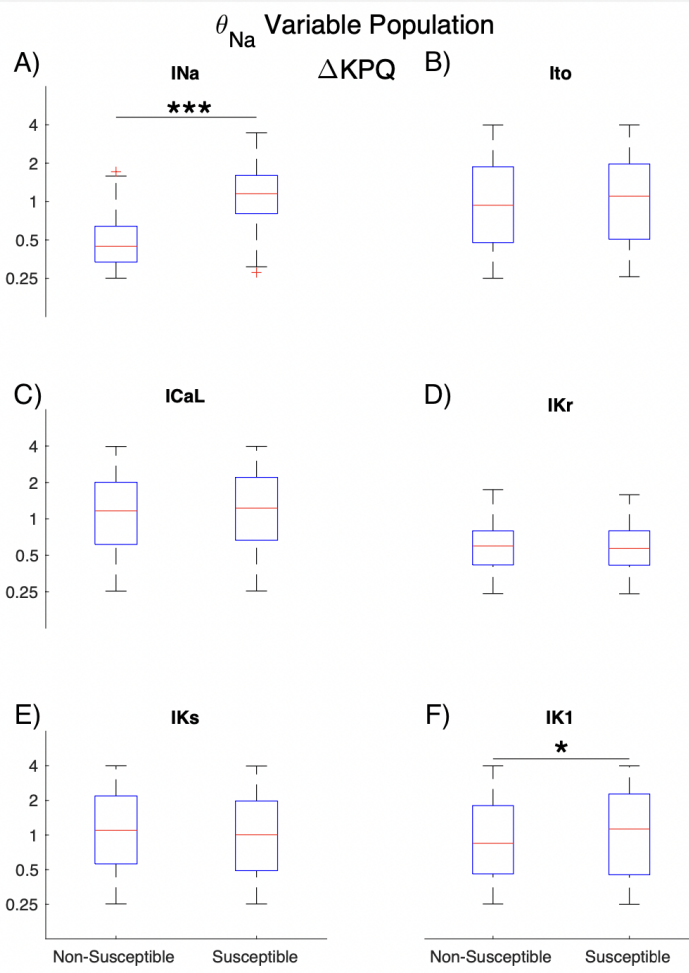


Figure S8. Boxplot illustrating difference in conductance scaling factor distributions for major currents, for the ΔKPQ mutation from the θ_{Na} variable population. We observe significant differences between susceptible and non-susceptible cells for θ_{Na} and θ_{K1} .

Supplemental figures from the fixed θ_{Na} population

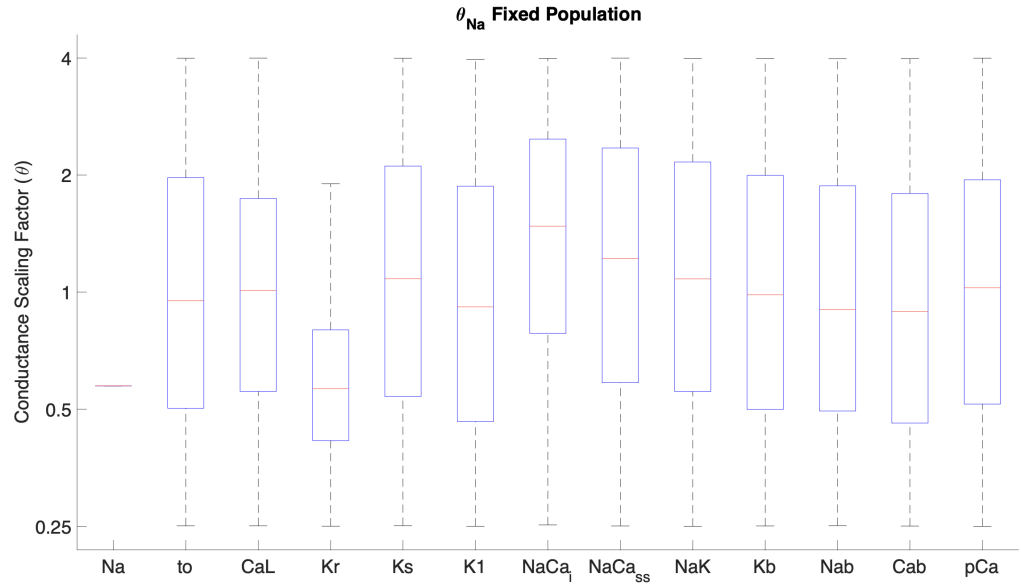


Figure S9. Distribution of current conductance scaling factors for the θ_{Na} fixed population. Note the θ_{Na} column is a single value, due to θ_{Na} fixed at the median value from the variable θ_{Na} population for all cells.

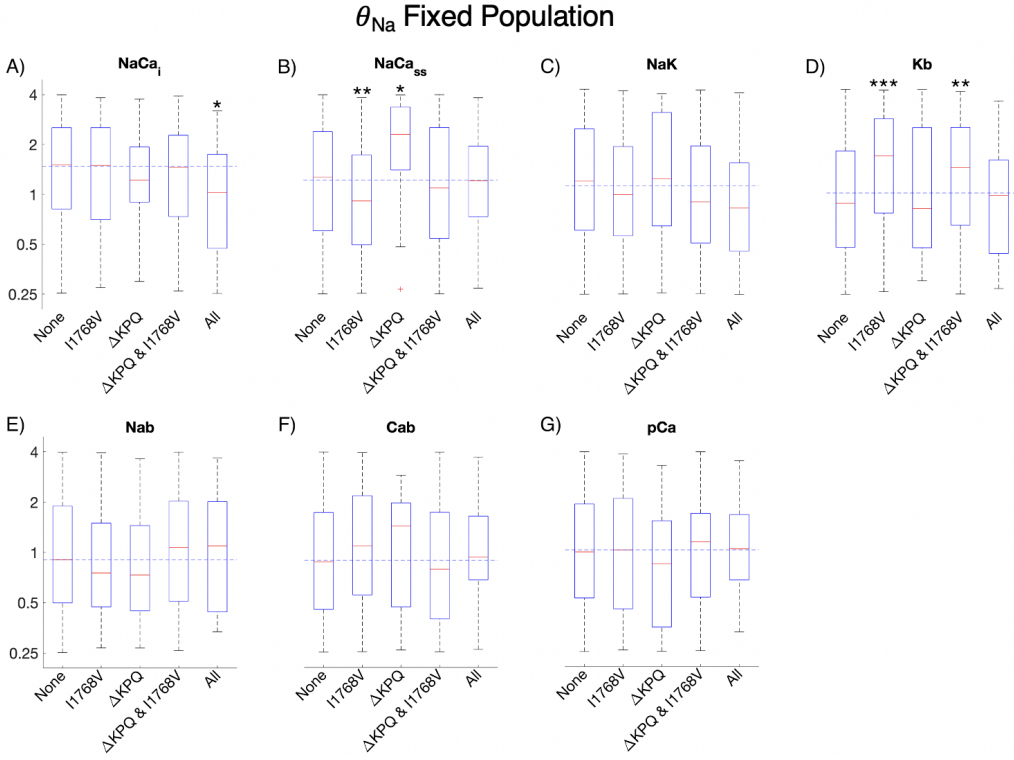


Figure S10. Relationship of conductance and susceptibility in θ_{Na} fixed population, plotted on a logarithmic scale. Trends are shown for currents not included in the main text. Significance is in reference to the sub-population of cells susceptible to no mutation. Distribution of I_{NaK} , I_{Nab} , I_{Cab} and I_{pCa} , shown in (C), (E), (F), and (G), respectively, show no significant difference between susceptible and non-susceptible sub-groups. (A) illustrates that cells susceptible to all mutations tend to have a lower intracellular sodium-calcium exchanger (I_{NaCa_i}) conductance. In (B) cells susceptible to only I1768V tend to have lower sub-space sodium-calcium exchanger ($I_{NaCa_{ss}}$) conductance while those susceptible to ΔKPQ only typically have elevated conductance. In (D), cells susceptible to only I1768V or both I1768V and ΔKPQ typically have a higher conductance for the background potassium current, I_{Kb} .

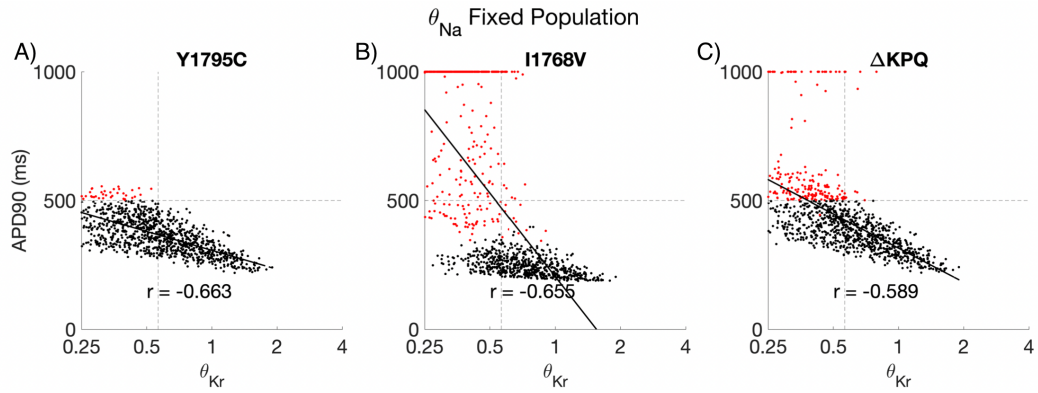


Figure S11. Relationship between θ_{Kr} and APD90 in cells with (A) Y1795C, (B) I1768V, and (C) ΔKPQ mutations, respectively, in the θ_{Na} fixed population. Population median is represented by the dashed horizontal line. Because θ_{Na} is constant, variable θ_{Kr} is comparable to a variable ratio of $\theta_{Kr}-\theta_{Na}$, investigated in the variable θ_{Na} population (Fig. S4B).

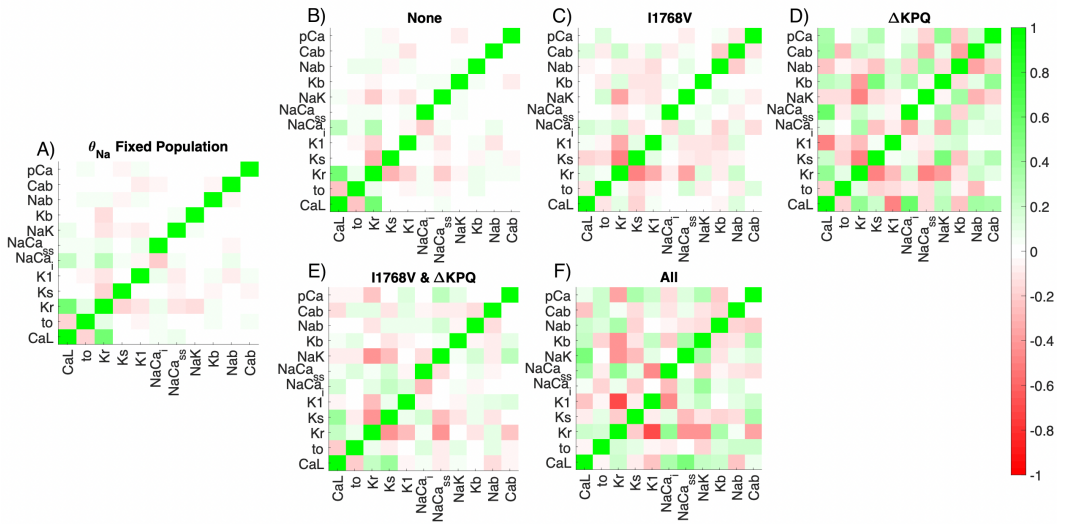


Figure S12. Pearson's correlation coefficient between pairs of all varied current conductances in the θ_{Na} fixed population. Dark red indicates a strong negative correlation, lack of color (white) indicates no correlation, and bright green indicates strong positive correlation. Correlation coefficients between current conductance for (A) the whole generated population, (B) cells susceptible to no mutations, (C) cells susceptible to I1768V only, (D) cells susceptible to ΔKPQ only, (E) cells susceptible to I1768V and ΔKPQ , and (F) cells susceptible to all mutations.

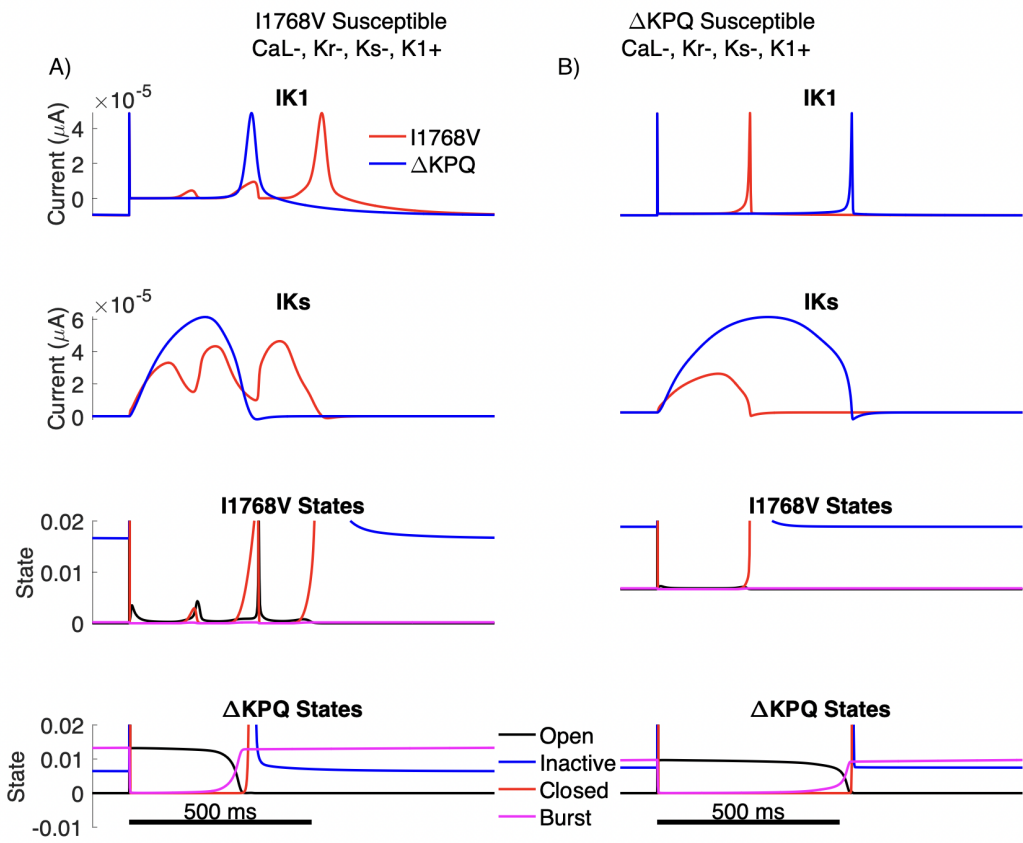


Figure S13. Traces for I_{K1} , I_{Ks} , and the I_{Na} Markov states corresponding to the cells and time shown in Fig. 13. (A) Example traces from the sample individual susceptible to I1768V only. (B) Example traces from the sample individual susceptible to ΔKPQ only. From top to bottom: I_{K1} , I_{Ks} , I_{Na} Markov chain states for the cell modeled with the I1768V mutation, I_{Na} Markov chain states for the same cell modeled with the ΔKPQ mutation.

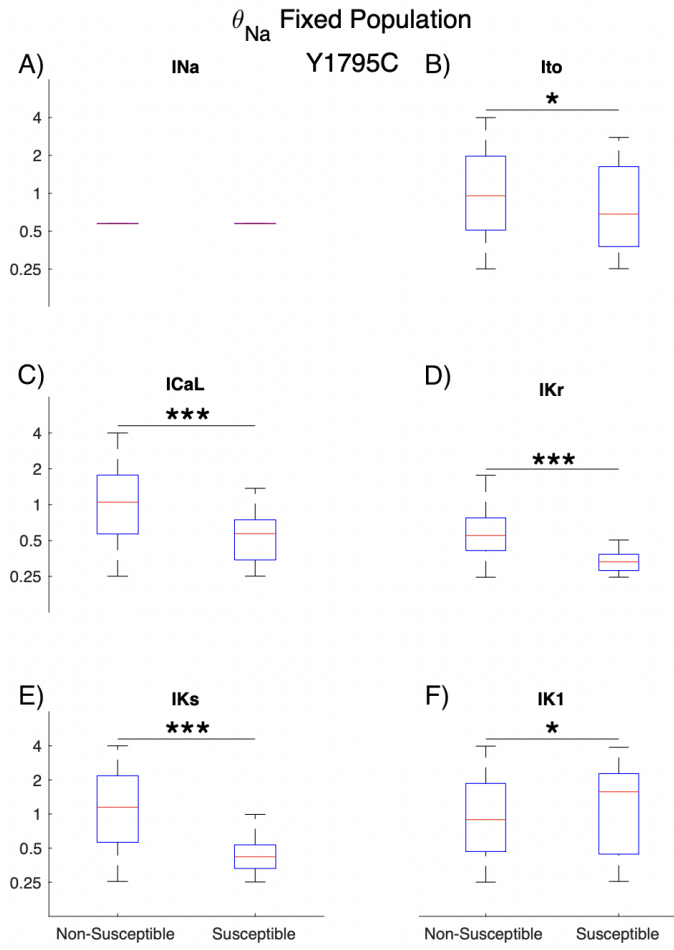


Figure S14. Boxplot illustrating difference in conductance scaling distribution for major currents, for the Y1795C mutation from the θ_{Na} fixed population. For fixed θ_{Na} , we see a similar trend for I_{Ks} (E) and I_{K1} (F). However, while no difference in the variable θ_{Na} population for I_{to} (B) and I_{CaL} (C), for fixed θ_{Na} , we observe a significant decrease in scaled conductance in the susceptible population for each (c.f., Fig. S6). We also observe a change in the trend for I_{Kr} (D).

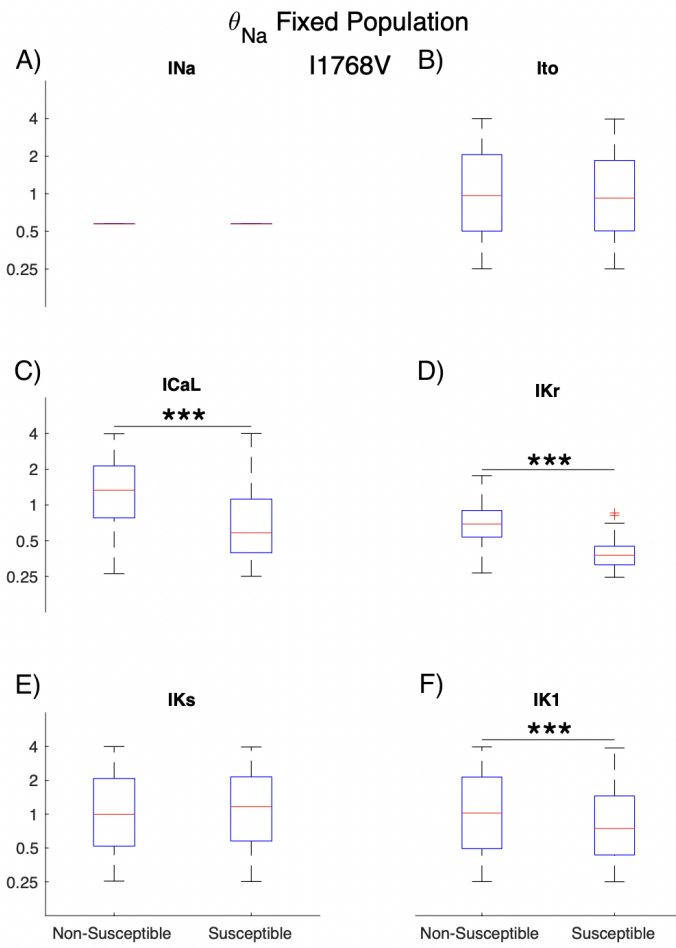


Figure S15. Boxplot illustrating difference in conductance scaling distribution for major currents, for the I1768V mutation from the θ_{Na} fixed population. Trends remain the same compared to the initial θ_{Na} variable population for all major scaled currents (Fig. S7).

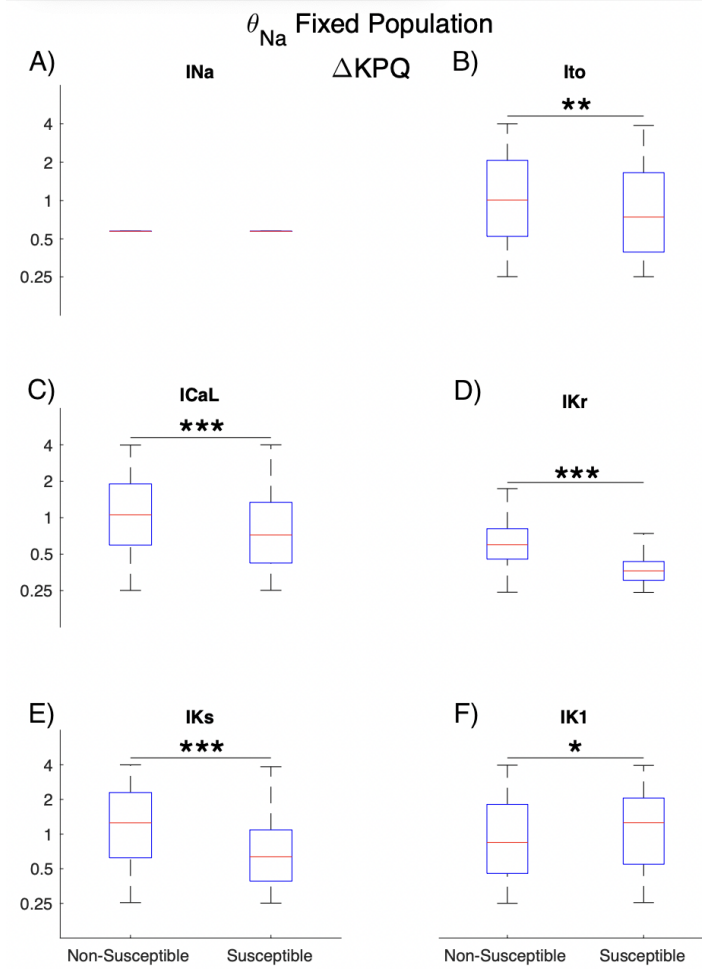


Figure S16. Boxplot illustrating difference in conductance scaling distribution for major currents, for the ΔKPQ mutation from the θ_{Na} fixed population. While the θ_{Na} variable population exhibited a lack of correlation between non-susceptible and susceptible sub-groups for I_{to} , I_{CaL} , I_{Kr} , and I_{Ks} (Fig. S8), for the fixed θ_{Na} population, we observe a significant decrease in the conductance coefficient for each of these currents in the sub-group of individuals susceptible to the mutation. Additionally, there is an observed increase in the distribution of I_{K1} .

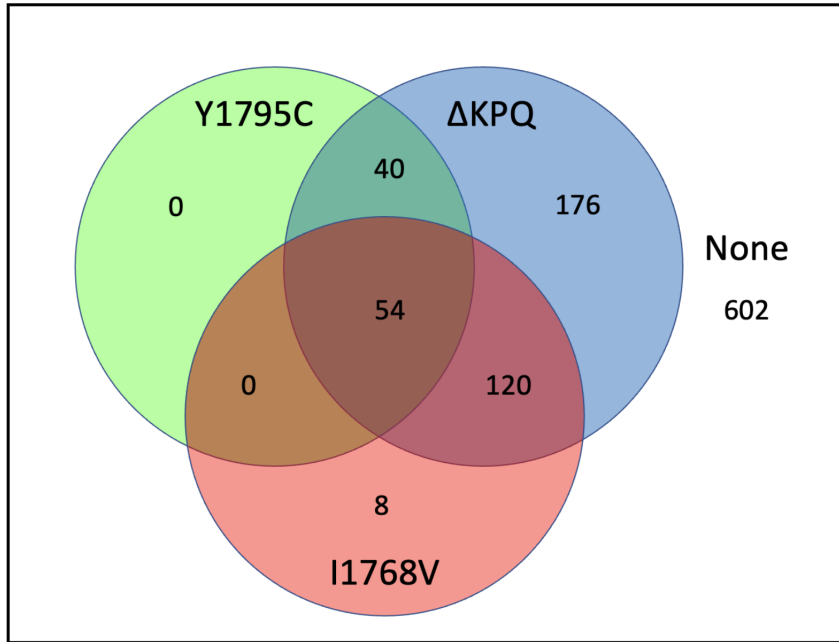


Figure S17. Venn diagram illustrating susceptibility categorization for all three mutations using the TNNP model. The TNNP model-generated population has similar overall susceptibility compared to the population simulated with the ORd model.

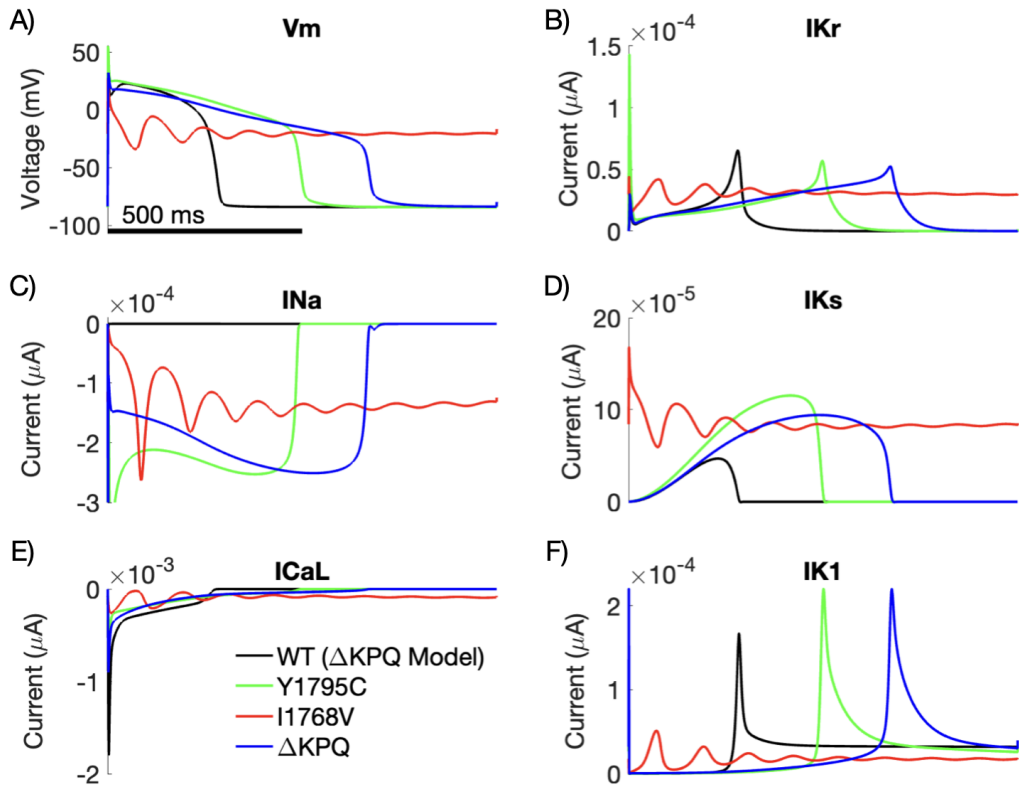


Figure S18. Example cell simulated using the TNNP model susceptible to all mutations with WT shown for reference. (A) Transmembrane voltage; (B) the rapid delayed potassium rectifier current, I_{Kr} ; (C) the sodium current, I_{Na} ; (D) the slow delayed rectifier potassium current, I_{Ks} ; (E) the long-lasting calcium current, I_{CaL} ; and (F) the inwardly rectifying potassium current, I_{K1} are shown as functions of time. Note that the cell with the I1768V mutation fails to repolarize.

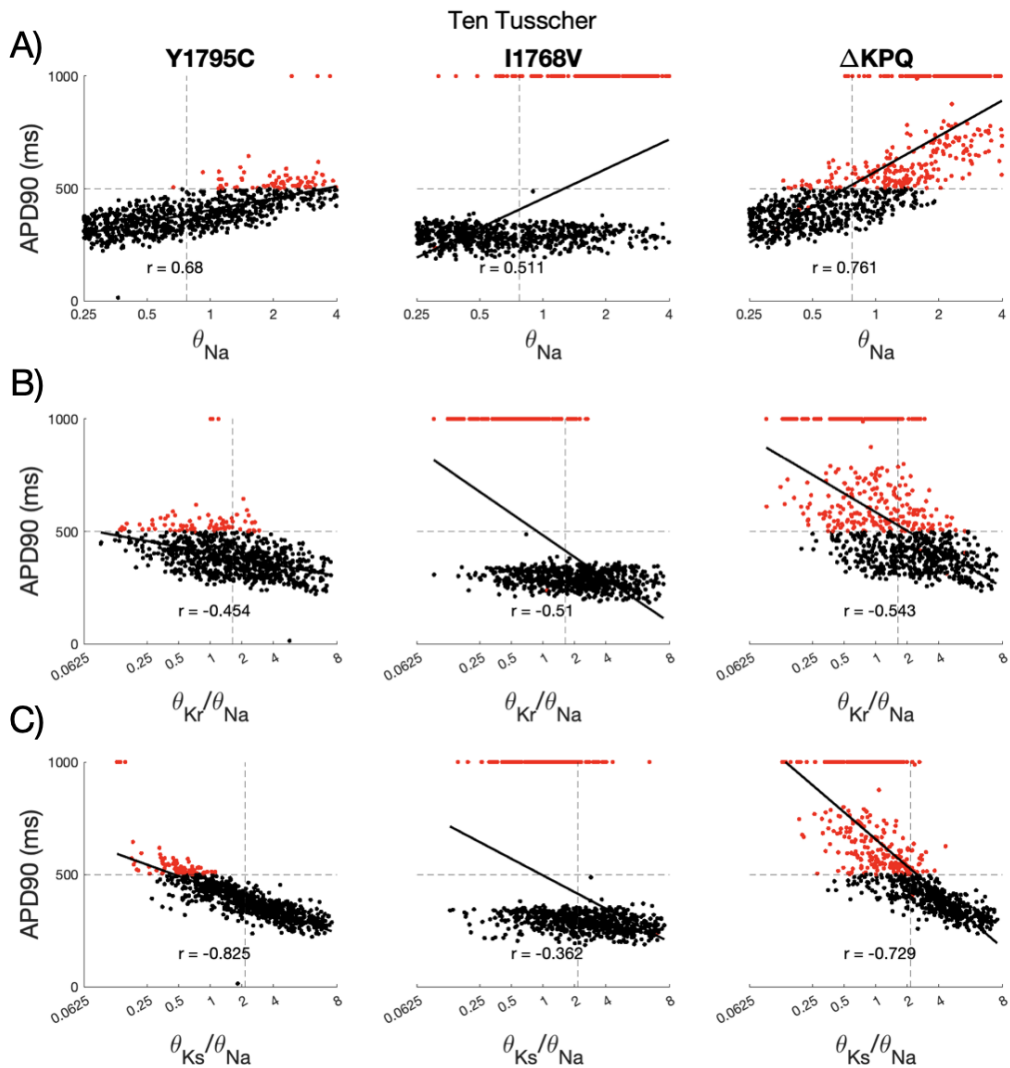


Figure S19. Correlation between major channel conductances and APD90 in virtual cells modeled with the ten Tusscher et al. (TNNP) model. (A) APD90 dependence on θ_{Na} shows a strong positive correlation in Y1795C and ΔKPQ , but not in I1768V. (B) The correlation between ratio of θ_{Kr} and θ_{Na} and APD90 leads to weaker correlations, compared with θ_{Na} alone, for cells with the Y1795C and ΔKPQ , and comparably poor correlation for cells with the I1768V mutation. (C) In contrast, the correlation between the θ_{Ks} - θ_{Na} ratio and APD90 is stronger, compared with θ_{Na} alone or the θ_{Kr} - θ_{Na} ratio, for cells with the Y1795C and ΔKPQ , while correlation is weak for cells with the I1768V mutation (as for θ_{Na} alone or the θ_{Kr} - θ_{Na} ratio). Horizontal dashed line shows the APD90 threshold for cells to be considered susceptible to a mutation. Vertical dashed line indicates the median value of θ_{Na} , θ_{Kr}/θ_{Na} , and θ_{Ks}/θ_{Na} in A-C, respectively. Pearson's correlation coefficient (r) is shown, with the line of best fit shown in solid black.

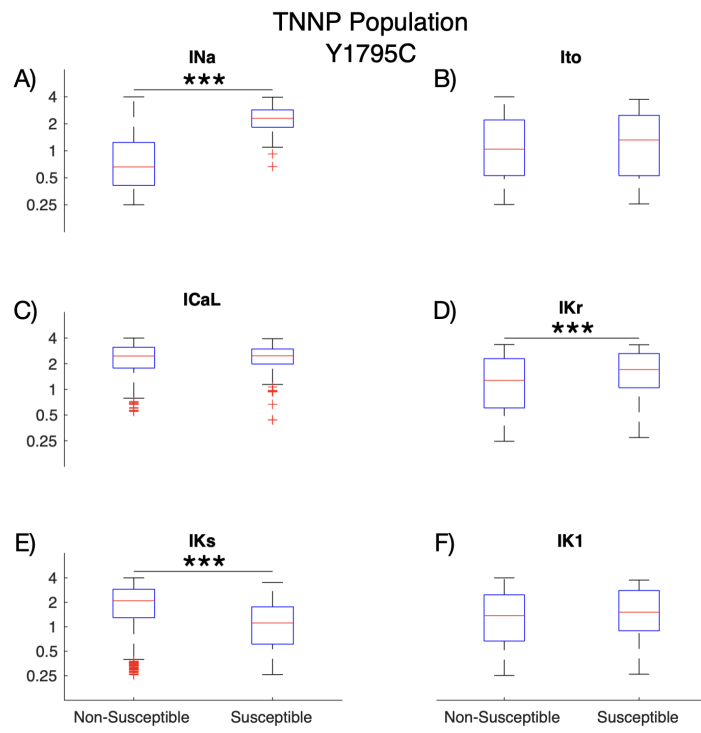


Figure S20. Boxplot illustrating difference in conductance scaling factor distributions for major currents, for the Y1795C mutation from the TNNP population. We observe significant differences between susceptible and non-susceptible cells for θ_{Na} , θ_{Kr} , and θ_{Ks} .

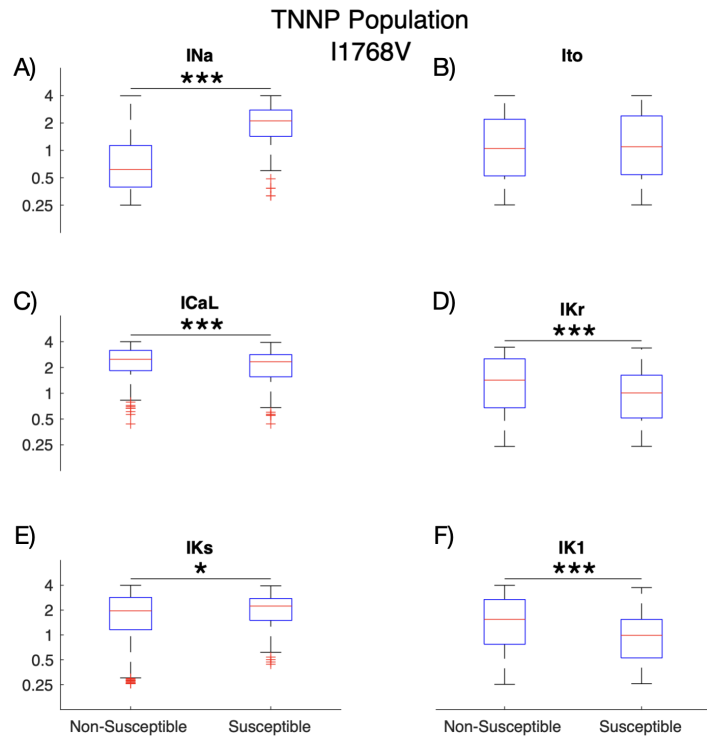


Figure S21. Boxplot illustrating difference in conductance scaling factor distributions for major currents, for the I1768V mutation from the TNNP population. We observe significant differences between susceptible and non-susceptible cells for θ_{Na} , θ_{CaL} , θ_{Kr} , θ_{Ks} , and θ_{K1} .

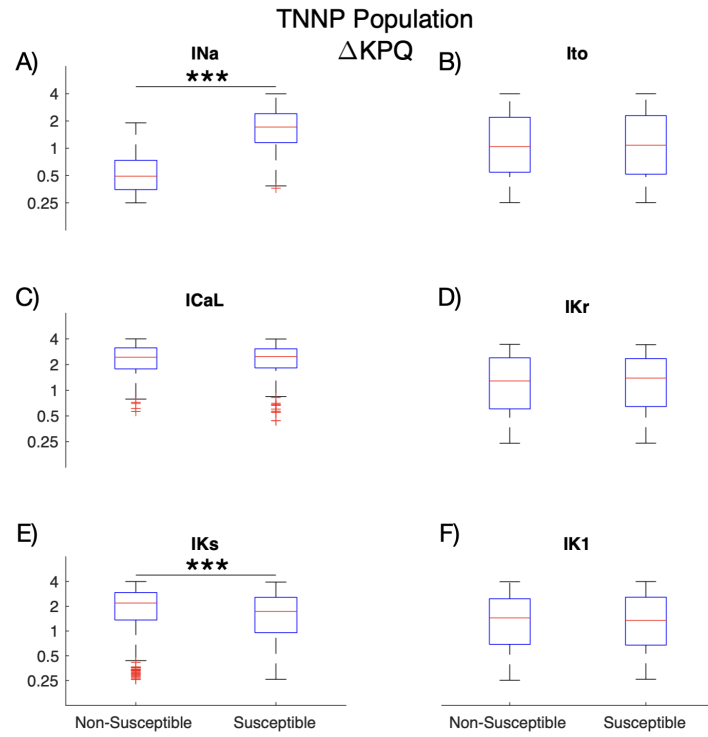


Figure S22. Boxplot illustrating difference in conductance scaling factor distributions for major currents, for the ΔKPQ mutation from the TNNP population. We observe significant differences between susceptible and non-susceptible cells for θ_{Na} and θ_{Ks} .